Science of Sintering, **45** (2013) 69-78

doi: 10.2298/SOS1301069M

UDK 676.017.5

Sol-gel as a Method to Tailor the Magnetic Properties of $Co_{1+y}Al_{2-y}O_4$

D. Milivojević[1*)], B. Babić-Stojić[1], V. Jokanović[1], Z. Jagličić[2], D. Branković[1], N. Jović[1], B. Čolović[1], S. Čupić[1], D. Kojić[3]

[1]Vinča Institute of Nuclear Sciences, University of Belgrade, P.O.Box 522, 11001 Belgrade, Serbia

[2]Institute of Mathematics, Physics and Mechanics, Jadranska 19, 1000 Ljubljana, Slovenia

[3]Faculty of Mechanical Engineering, University of Belgrade, Kraljice Marije 16, 11120 Belgrade, Serbia

Abstract:

The magnetic properties of mesoscopic materials are modified by size and surface effects. We present a sol-gel method used to tailor these effects, and illustrate it on $Co_{1+y}Al_{2-y}O_4$ spinel. Nanocomposites made of spinel oxide $Co_{1+y}Al_{2-y}O_4$ particles dispersed in an amorphous SiO_2 matrix were synthesized. Samples with various mass fractions -x of $Co_{1+y}Al_{2-y}O_4$ in composite, ranging from predominantly SiO_2 (x = 10 wt%) to predominantly spinel (x = 95 wt%), and with various Co concentrations in spinel y were studied. The spinel grain sizes were below 100 nm with a large size distribution, for samples with predominant spinel phase. Those samples showed Curie-Weiss paramagnetic behavior with antiferromagnetically interacting Co ions ($\theta \approx -100$ K). The grain sizes of spinel stays confined in 100 nm range even in the spinel samples diluted with as low as 5 wt% concentration of amorphous SiO_2. For the samples with predominant SiO_2 the crystalline nanoparticles are well separated and of size of around 100 nm, but with presence of much smaller spinel nanoparticles of about 10 nm. The magnetic properties of the samples with predominant silica phase showed complex behavior, spin-glass magnetic freezing at the lowest temperatures and lower absolute value of θ and consequently lower exchange constant.

Keywords: *Magnetic materials; Sol-gel preparation; Nanocomposites; Spin glass; Magnetic properties.*

1. Introduction

$Co_{1+y}Al_{2-y}O_4$ belongs to the group of magnetic spinel oxides (represented with the general formula AB_2O_4). The spinel crystal lattice is a cubic with a face centered (f.c.c.) packing of oxygen atoms which form tetrahedral (A) and octahedral (B) holes (sites) occupied by cations. In the so-called normal spinels, the A site is occupied by divalent cation (M), while the B site is filled by trivalent cation (N). Generally, the cations distribution is random and can be represented by the formula $(M_{1-\delta}N_{\delta})_{tet}[M_{\delta}N_{2-\delta}]_{oct}O_4$ where δ denotes the inversion parameter and can take any value $0 \leq \delta \leq 1$. In an inverse spinel, $\delta = 1$. Both, A and B sites,

*) **Corresponding author**: dusanm@vinca.rs

can accommodate magnetic cations and in that case there is the competition between various types of superexchange interaction (J_{AA}, J_{BB}, and J_{AB}). Hence, variation of the magnetic cations distribution over the A and B sites can provoke different magnetic behavior in spinel compounds.

Bulk Co_3O_4 is the normal spinel ($\delta = 0$) with the magnetic moment equal to magnetic moment of Co^{2+} in A position. Co^{3+} in B position is in low-spin state with no magnetic moment [1]. In bulk $Co_{1+y}Al_{2-y}O_4$, Co preferentially takes the A position [2]. Polycrystalline $CoAl_2O_4$ shows spin-glass (SG), while $CoCo_2O_4$ shows antiferromagnetic (AF) ground state at the lowest temperatures. Intermediate $CoCoAlO_4$ shows spin-liquid state [2-4].

Behavior of magnetic materials in reduced dimensions is a very interesting topic both for fundamental research and for application in spintronics. Magnetic properties of nanoparticles are greatly determined by surface effects, particularly antiferomagnetics. By decreasing particle size to nano dimensions, the finite size effects give rise to surface spin canting, superparamagnetism (SPM), and/or site disorder effect. Many factors determine magnetic behavior of nanosized system, like particle size and shape, size distribution, agglomeration, cation distribution, interparticle interactions. As magnetic nanoparticles usually tend to agglomerate due to their large surface energy and/or strong magnetic interactions, it is useful to study their magnetic properties in the form of nanocomposites. In this work we used sol-gel method to explore the influence of different level of dilution in amorphous silica matrix, ranging from predominantly SiO_2 (x = 10 wt%) to predominantly spinel (x = 95 wt%), where x is mass fraction of $Co_{1+y}Al_{2-y}O_4$ in composite. Various Co concentration in spinel, y, were also studied.

2. Experimental details

Nanocomposites were synthesized by the sol-gel technique. The basic idea, considering different silica:spinel ratio, is illustrated in Fig. 1. The left branch illustrates synthesis with predominant silica and right branch illustrates nanocomposite with predominant spinel.

Tetraethylorthosilicates (TEOS) [$Si(C_2H_5O)_4$] was used as a precursor for the SiO_2, whereas cobalt nitrate hexahydrate [$Co(NO_3)_2{\cdot}6H_2O$] and aluminium nitrate nonahydrate [$Al(NO_3)_3{\cdot}9H_2O$], were used as precursors for the $Co_{1+y}Al_{2-y}O_4$ nanoparticles. A cold mixture of HCl and water in the molar ratio 0.01:1 is added dropwise to a cold mixture of TEOS and ethanol in the volume ratio 1:1, under vigorous stirring. The molar water : TEOS ratio was set to be 4:1. So obtained silica sol was used as a silica precursor for the next step of synthesis. In the next step, the mixture of $Co(NO_3)_2{\cdot}6H_2O$ and $Al(NO_3)_3{\cdot}9H_2O$ solutions in deionised water was added dropwise to the obtained silica sol solution corresponding to various x and y ratios (see Table I). Further, the total amount of water was adjusted to be 8 molecules of water per one molecule of TEOS monomer.

The 2 M solution of ammonia [NH_4OH] was dropped inside of this mixture until the pH value was set up to be 7. NH_4OH enable transformation of Co precursor into corresponding Co-ammino complexes ($[Co(NH_3)_{6-n}(H_2O)_n]^{2+}$, $[Co(NH_3)_{6-n}(H_2O)_n]^{3+}$) and Al precursors to $Al(OH)_3$. The point of zero charge of $Al(OH)_3$ is at about pH = 9.7 (maximum zeta potential of aluminum hydroxide is at about 4.5) and higher values of pH cause its faster precipitation [5]. Yet again, the higher concentration of ammonia has opposite impact on solubility of Co complexes.

Therefore, the amount of added NH_4OH should be adjusted to be as more as close to balanced kinetics of precipitation of $Al(OH)_3$ and Co ammine complex. The value of pH = 7 seems to be optimal for balanced precipitation. The formation of single Co_Al oxide phase without phase separation, diluted inside of SiO_2 phase, confirms that the given pH is indeed chosen properly.

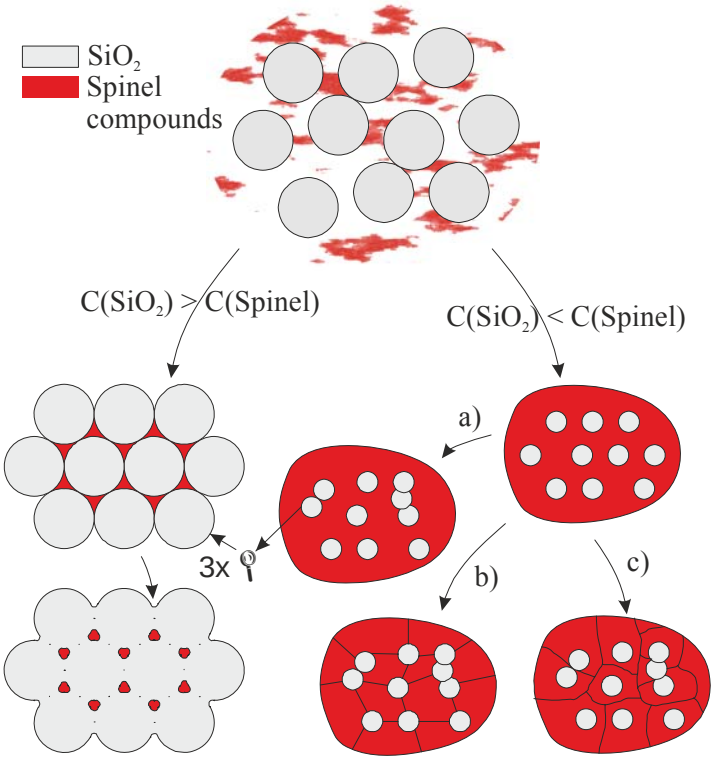

Fig. 1. Synthesis diagram.

The mixture was then placed in an oven at 50°C for 24 h in order to complete the gelling. Before final gelling, a reaction of Co amino complex degradation (caused by ammonium evaporation) occurs. This process is followed with slight change of color from ocher to the dark reddish brown, due to partial change of valence of Co ions. As obtained complex gel was then dried at 150°C for three days, and annealed at 550°C for 5 hours in air.

The compositions of obtained samples were determined by atomic absorption method. The samples were labeled according to mass fraction x of $Co_{1+y}Al_{2-y}O_4$ in composite, and y as Sx_y (Table I).

Powder X-ray diffraction (XRD) spectra were recorded on a Philips 1710 diffractometer using CuK_α radiation without energy filters, with a step size (2θ) of 0.05° at a slow scan rate of 40 s per step. The magnetization measurements were carried out on a SQUID magnetometer (MPMS XL-5, Quantum Design). The dc magnetization measured at H = 8, 50, 100, 1000 and 10000 Oe under zero-field-cooled (ZFC) and field-cooled (FC) regimes, were recorded in the range of temperature from 2 K to 300 K. The ac magnetization measurements were made under an ac exciting field of 6.5 Oe, in the frequency range from 1 to 1500 Hz. The hysteresis loop, M(H) curves, were recorded at 2, 5, 10, 20 and 50 K. Transmission electron microscopy (TEM) micrographs were obtained using a JEOL 2010 F microscope operating at 200 kV coupled with an EDXS microanalysis system (LINK ISIS EDS 300). Finely ground samples were dispersed in ethanol, then submitted to ultrasonic bath and the as-obtained suspension was placed on carbon coated copper grids. Atomic force microscopy (AFM) was carried out in AC-tapping mode in ambient air using a JSPM-5200 JEOL instrument. The samples were obtained by pressing powder into pellets.

3. Results
Morphology and microstructure

The morphology of the samples was imaged using atomic force microscope, AFM, phase-contrast technique (in tapping mode and in ambient air). AFM systems are able to detect intermolecular forces in the order of 10^{-11} – 10^{-13} N which belong to the class of van der Waals type forces, usually modeled by Lennard-Jones potentials (LJP). The variations in the slopes of LJP curves (typical for each chemical species) determine different intermolecular forces acting on the AFM sensor tip. That difference modulates the vibration frequency of the AFM cantilever, creating a higher-harmonics in the feedback signal of AFM system. The varying magnitudes of higher-harmonics are the signals detected and displayed in phase-contrast images. In our case, they depict the difference between force fields of matrix material (SiO_2) and nano-structured filling material, thus visualizing the grain border which enables us to deduce the sizes of different grains.

Observed grain sizes show significant variation in the range below 100 nm (20 – 100 nm) (Fig. 2). The sizes are 20-60 nm for the sample with 56 wt% of the spinel, 30-100 nm for the 75 wt% and 30-110 nm for the sample with 95 wt% concentration of spinel. The fraction of grains ≥100 nm is small and subject to possible merging of smaller grains. It can be concluded that grain sizes are larger for the higher concentration of spinel. It is interesting to note that grain sizes of spinel stays confined in 100 nm range even in the samples diluted with as low as 5 wt% concentration of amorphous SiO_2. Regarding the fact that silica has a density of 2.2 g/cm^3, much lower than that of Al-substituted Co_3O_4 (~ 5.6 g/cm^3), the corresponding volume percentages of spinel are lower.

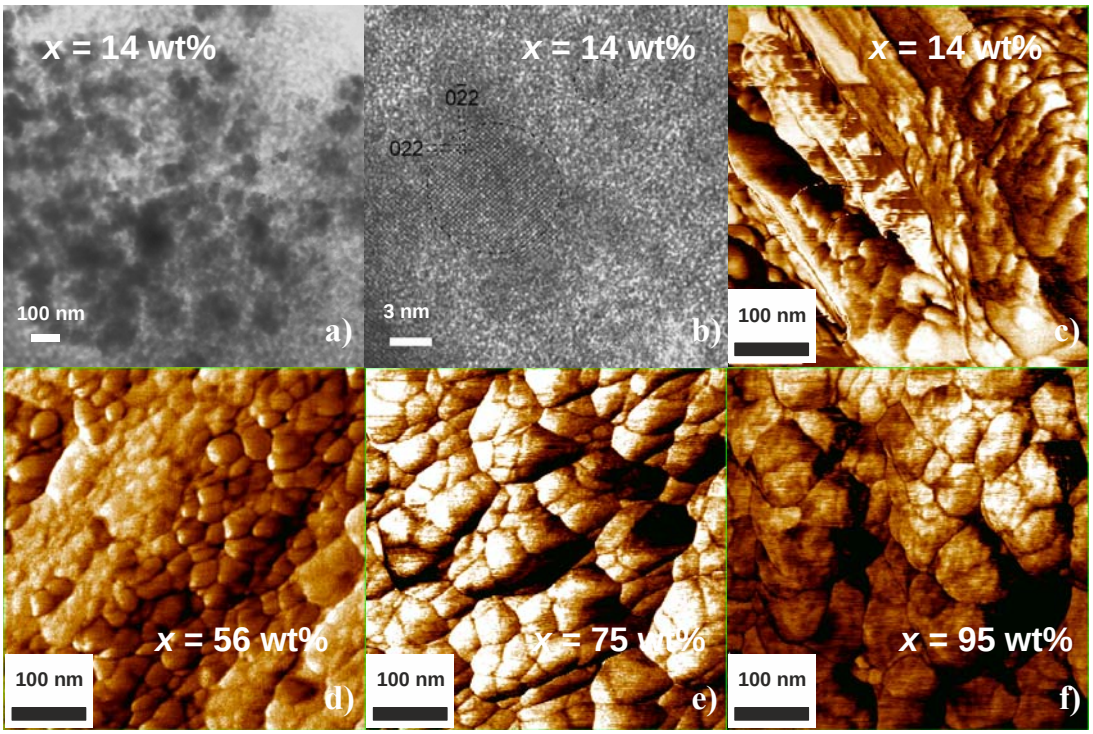

Fig. 2. a), b) TEM micrographs of the sample S1_13. AFM phase-contrast micrographs of samples c) S1_13, d) S5_09, e) S7_12 and f) S9_13.

The possible mechanism of confinement of grain growth is illustrated in C(SiO_2)<C(spinel) branch in Fig. 1. The mechanism illustrated with branch a), where spinel grows as there is no

SiO_2 and SiO_2 acts only as some kind of impurity, is not valid. The grains observed in AFM, Fig 2, x = 56, 75 and 95 wt%, could be formed by the mechanisms shown in branches b) or c). The branch b) illustrates the possibility that the spinel nucleation centres form between the sol particles and the SiO_2 particles stops grain growth. The branch c) illustrate possibility that silica colloidal particles behaves as a substrate and nucleation centres for the spinel grain growth. On the other side, for the samples with prevailing amorphous SiO_2 phase, the distinctive grains are hardly visible, shapeless (amorphous) mass prevail. The samples with prevailing SiO_2 phase are analyzed by TEM. In vast majority, the crystalline nanoparticles are well separated and of size around 100 nm (Fig. 2(a)), however, TEM reveals presence of much smaller structures, with size below 10 nm in sample S1_13 (Fig. 2(b)). The sizes of amorphous SiO_2 particles range from 14 to 50 nm.

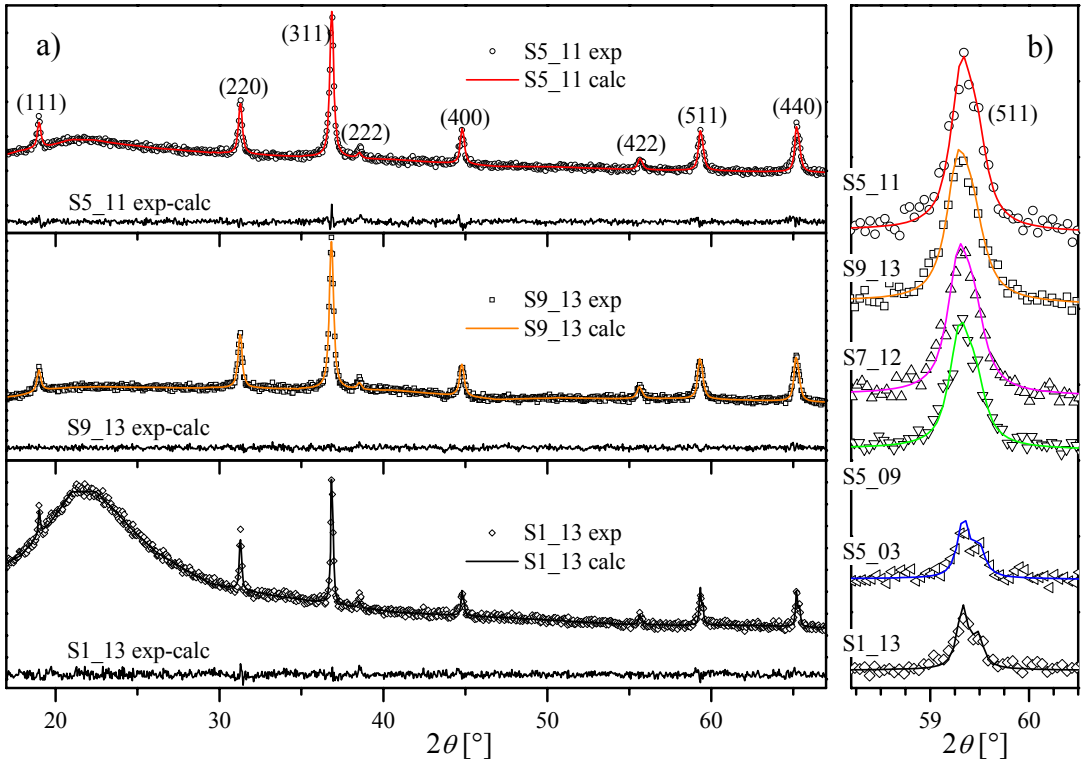

Fig. 3. a) XRD experimental patterns (exp), Rietveld analysis calculated spectra (calc) and their difference for the samples S5_11, S9_13 and S1_13, b) Zoom of the (511) diffraction peak for all the samples (symbols – experimental, lines - calculated).

XRD patterns (Fig. 3) of the studied samples show the broad reflection centered at 21.5° originating from amorphous silica matrix, and the narrow diffraction peaks that correspond to cubic spinel phase (space group Fd3-m). Presence of any impurity phase was not found. The spectra were fitted using FullProf-program based on the Rietveld method (Fig. 3). Linear interpolation with 19 points was used to describe background. Relatively high background comes from diffraction from amorphous SiO_2 and from fluorescence when Cu cathode is used (no energy filter was used). Peak profiles were delineated by Pseudo-Voigt peak shape function. The crystallite sizes calculated from the XRD line broadening range from 30 to 90 nm. The width of the diffraction lines is illustrated with enlarged peak (511) shown in Fig. 3(b). The crystallite sizes obtained from XRD agree well with grain sizes observed using AFM. The occupation factors were fitted taking into account Co-Al ratio

determined by atomic absorption method. The occupation factors can be accurately determined because relative intensity of diffraction peaks greatly depends on occupation factors. The obtained occupation factors of Co in A position - Co/A, $\left(Co^{2+}_{Co/A}Al^{3+}_{1-Co/A}\right)_A\left[Co^{3+}_{y}Co^{2+}_{1-Co/A}Al^{3+}_{2-y-(1-Co/A)}\right]_B O_4$, are given in Table I. The samples do not show significant preference of Co to A position. The fraction of Co ions at A position, (Co/A)/(1+y), range from 0.33 to 0.38, which is close to random (0.33).

Tab. I Sample labels, y – composition of $Co_{1+y}Al_{2-y}O_4$, x – mass fraction of $Co_{1+y}Al_{2-y}O_4$ in composite, T_f – positions of peaks of χ''(T) at f = 1 Hz, $\Phi = \Delta T_f/(T_f \Delta \log f)$ – frequency shift of respective values from column T_f, Co/A, Co/B, (Co/A)/(1+y) – fraction of Co at specified position, p_{eff} – effective magnetic moment per $Co_{1+y}Al_{2-y}O_4$ molecule, θ– Curie-Weiss temperature, M(50 kOe, 2 K) – magnetization at H = 50 kOe and T = 2 K, H_c – coercive field at T = 2

Label	y	x [wt%]	T_f [K]	↔ Φ	Co/A	Co/B	(Co/A)/ /(1+y)	p_{eff} [μ_B]	θ [K]	M(50 kOe, 2 K) [μ_B/mol]	H_c(2 K) [Oe]
S1_13	1.32	14	5.1, 8.9	↔ 0.08, ↔ 0.08	0.87	1.45	0.375	4.52	-23	0.93	1050
S7_12	1.20	75	5.2	↔ 0.11	0.81	1.38	0.368	4.39	-108	0.25	140
S9_13	1.34	95	5.7, 11.1	↔ 0.08, f ≤ 500 Hz ↔ 0.06	0.85	1.49	0.363	4.25	-84	0.27	180
S5_03	0.30	50	3.6	↔ 0.10	0.44	0.87	0.338	3.80	-46	0.60	100
S5_09	0.93	56	5.4	↔ 0.07	0.72	1.21	0.373	4.28	-98	0.31	110
S5_11	1.07	55	3.0, 6.4	↔ 0.10, ↔ 0.07	0.71	1.36	0.343	4.72	-76	0.44	540

Magnetic measurements

Magnetic susceptibility at higher temperatures was analyzed using the Curie-Weiss (CW) equation, $\chi = Np_{eff}^2/(3k_B(T-\theta))$ (Table 2), where N is the number of $Co_{1+y}Al_{2-y}O_4$ molecules per unit mass, θ is the Curie-Weiss temperature and p_{eff} is the effective magnetic moment per $Co_{1+y}Al_{2-y}O_4$ molecule. Fig. 4 shows inverse susceptibility χ^{-1} vs temperature for various samples. Three of the samples, S5_09, S9_13 and S7_12, with higher concentration of $Co_{1+y}Al_{2-y}O_4$ in SiO_2, behave as Curie-Weiss paramagnets with antiferromagnetically interacting Co ions (θ ≈ -100 K). The negative θ points to prevailing antiferromagnetic interaction.These samples show similar χ(T) dependencies (Fig. 4). Other three samples, with higher concentration of silica S1_13, S5_03 and S5_11 show lower absolute value of θ (Table I).

The value of the Curie-Weiss temperature θ represents the strength of the leading exchange interaction. The obtained lower absolute values of θ (Table 1) of the samples with higher concentration of silica S1_13, S5_03 and S5_11 than reported values [1, 6, 7, 8] points to decrease in the strength of the antiferromagnetic exchange interactions between the Co ions or onset of ferromagnetic interaction that competes with antiferromagnetic.

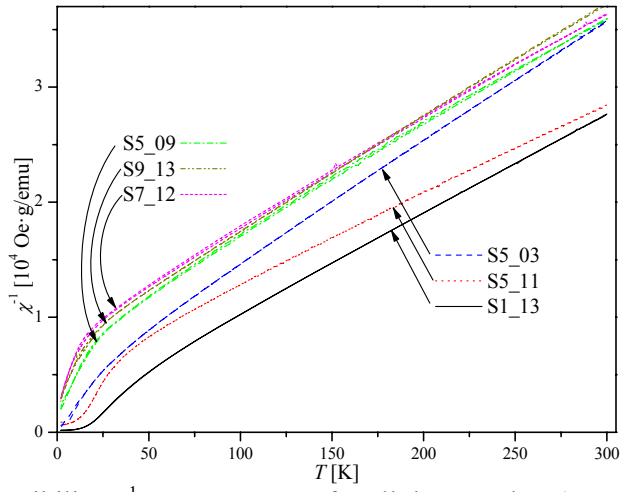

Fig. 4. Inverse susceptibility χ^{-1} vs temperature for all the samples. (note: the susceptibility is per gram of $Co_{1+y}Al_{2-y}O_4$).

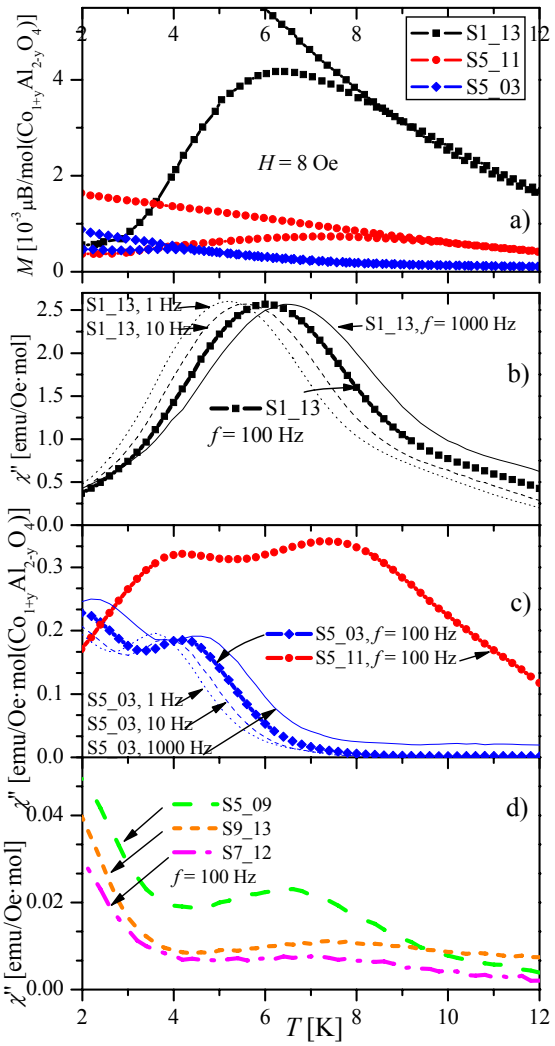

Fig. 5. a) ZFCFC M(T) curves of samples S1_13, S5_03 and S5_11. b), c), d) Imaginary part of the ac magnetic susceptibility χ" per mole of $Co_{1+y}Al_{2-y}O_4$ as a function of temperature b) for sample S1_13, c) for samples S5_03 and S5_11 and d) for S5_09, S7_12 and S9_13.

ZFCFC curves of the samples S1_13, S5_03 and S5_11 show bifurcation (Fig. 5(a)). Bifurcation of the FC and ZFC branches in the dc magnetic susceptibility is characteristic of most of the spin-glass systems, but also of the interacting and non-interacting superparamagnetic nanoparticles. Absence of the ZFCFC bifurcation and hardly detectable ac susceptibility peaks for the samples S5_09, S9_13 and S7_12, verify them as primarily Curie-Weiss paramagnetic down to 2 K.

Figs. 5 (b,c and d) show the temperature dependence of the imaginary part of the ac magnetic susceptibility χ''(T) for all the samples at frequencies f of ac applied magnetic field. Imaginary part of all the samples shows more or less distinctive peaks at very low temperatures (<12K). The positions of peaks observed in χ''(T) moves to higher temperatures with increasing frequency f . We used the empirical parameter $\Phi = \Delta T_f/(T_f \Delta \log f)$ to classify the origin of the observed maxima [9]. The values of the parameter Φ are presented in Table 1. The values are about 0.08 (0.07-0.10) except for the samples S9_13 and S7_12 which show higher values because peaks merge and disappear for frequencies higher than 50 Hz and positions cannot be determined precisely. If we waive the values for f > 50 Hz, we also get value of Φ_{S9_13} to be 0.08. These values are consistent with those for semiconducting and insulating spin glasses [9].

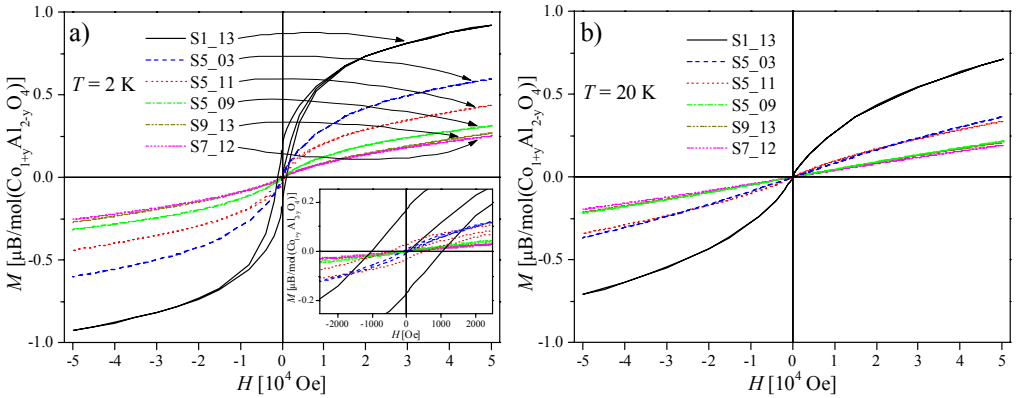

Fig. 6. Magnetization curves. a) T = 2 K, b) T = 20 K.

Fig. 6 shows magnetization curves at a) T = 2 K and b) T = 20 K. The same grouping of results (intensity of magnetization), considering concentration of $Co_{1+y}Al_{2-y}O_4$ in nanocomposite, can be observed, as were observed in static χ(T) and in dynamic χ''(T) magnetic susceptibility data. The magnetic frozen states and values of θ influence the M(H) behavior (M = f(T + θ)) and therefore is substantial difference of magnetization curves between various samples, especially between paramagnetic samples, S5_09, S9_13 and S7_12, and spin-glass samples, Fig. 6.

The magnetization curves M(H) at 50 K show Brillouin like curvature. At lower temperatures (≤20 K) the curves deviate from the Brillouin function. The M(H) curves show hysteresis at lower temperatures, below about 10 K. The sample S1_13 exhibits appreciable hysteresis with coercive field H_c around 1000 Oe at T = 2 K, and sample S5_11 shows coercive field around 540 Oe. All the other samples show an order of magnitude lower H_c (Table 1). At higher temperatures (≥5 K) the values of H_c are lower than 50 Oe for all the samples.

Pure bulk Co_3O_4 is antiferromagnetic with the Néel transition temperature T_N = 30 K [1, 6]. The χ(T) and χ''(T) dependencies of our samples show Curie-Weiss behavior and does not exhibit magnetic phase transition at 30 K. It is a system with strong frustration effect and emergence of frozen magnetic ground state is expected [2, 4]. The results suggest existence of magnetic ground states below temperature of magnetic ground state of bulk Co_3O_4, and even

more, existence of multiple magnetic ground states that can form at various temperatures. Analysis suggests that these states are of spin-glass type.

The strength and positions of the ac susceptibility peaks correspond to ZFCFC bifurcation extent and particularly to the intensity and position of the peaks at ZFC branch; (compare b) and c) to a) of Fig. 5). The sample with predominant silica, S1_13, show the strongest ac susceptibility peaks. The peaks of samples with medium concentration of silica, S5_03 and S5_11 are order of magnitude weaker and the samples with predominant $Co_{1+y}Al_{2-y}O_4$, S5_09, S9_13 and S7_12 show two orders of magnitude weaker ac susceptibility peaks. The samples with low intensity ac susceptibility peaks, S5_09, S7_12 and S9_13, do not show ZFCFC bifurcation.

The samples with more distinguished magnetic frozen state characteristic, (S1_13, S5_03, S5_11), also have markedly lower absolute values of θ and higher intensities of magnetization at the lowest temperature (Table 1, Fig. 6). Lower absolute values of negative θ point to decrease in the strength of the antiferromagnetic exchange interactions between the Co ions or onset of ferromagnetic interaction that competes with antiferromagnetic. Correlation of M and θ with x suggests surface physics as significant. We suggest a solid-state surface electrochemical reaction, described by Martin-Gonzales et al. [10] as responsible for behaviour of the magnetic properties of this material; Surface Co ions at A position may interact ferromagnetically at $Co_{1+y}Al_{2-y}O_4$ – SiO_2 interface, due to solid-state surface electrochemical reaction where SiO_2 reduces Co at B position from Co^{3+} oxidation state, that has zero magnetic moment, to Co^{2+}, with magnetic moment, and consequently the non-zero moment may appear due to A-O-B-O-A interaction.

The variation of Al concentration in polycrystalline $Co_{1+y}Al_{2-y}O_4$, with insignificant inversion, changes the Néel temperature T_N, but does not have substantial influence on θ [4]. In our samples no correlation between θ or T_f to inversion or Al concentration could be established.

Conclusion

Magnetic spinel oxide $Co_{1+y}Al_{2-y}O_4$ dispersed in an amorphous SiO_2 matrix synthesized by a sol-gel technique were studied. The used sol-gel method provided size confinement of the $Co_{1+y}Al_{2-y}O_4$ nanoparticles to be ≤ 100 nm even for the sample with as low as 5 wt% of silica. The Co and Al ions occupation of cation positions in spinel were close to random. The samples, with higher concentration x of $Co_{1+y}Al_{2-y}O_4$ in SiO_2 were Curie-Weiss paramagnets with antiferromagnetically interacting Co ions (θ ≈ -100 K). Other samples, with lower x, showed complex behavior, spin-glass magnetic freezing at the lowest temperatures and lower absolute value of θ associated with lower exchange constant.

Acknowledgements

Financial support for this study was granted by the Ministry of Science of the Republic of Serbia, project No 172026.

4. References

1. W. L. Roth, J. Phys. Chem. Solids, 25 (1964) 1.
2. N. Tristan, V. Zestrea, G. Behr, R. Klingeler, B. Buchner, H. A. Krug von Nidda, A. Loidl, V. Tsurkan, Phys. Rev. B, **77** (2008) 094412F.
3. A. Krimmel, V. Tsurkan, D. Sheptyakov, A. Loidl, Physica B, 378 (2006) 583.
4. O. Zaharko, A. Cervellino, V. Tsurkan, N. B. Christensen, A. Loidl, Phys. Rev. B, 81 (2010) 064416.

5. T. Žak, V. Ćosović, A. Ćosović, B. David, N. Talijan, D. Živković, Sci. Sinter., 44 (2012) 103
6. S. Goldberg, A. J. Davis, D. J. Hem, in: "The environmental chemistry of aluminum", 2nd, Eds. Garrison Sposito, CRC Lewis Publishers, Boca Raton New York London Tokyo, 1995, ch. 7.
7. P. Dutta, M. S. Seehra, S. Thota, J. Kumar, J. Phys.: Condens. Matter., 20 (2008) 015218.
8. A. Maljuk, V. Tsurkan, V. Zestrea, O. Zaharko, A. Cervelino, A. Loidl, D. N. Argyriou, J. Cryst. Growth, 311 (2009) 3997.
9. T. Suzuki, H. Nagai, M. Nohara, H. Takagi, J. Phys.: Condens. Matter., 19 (2007) 145265.
10. J. A. Mydosh, Spin Glasses: an Experimental Introduction., Taylor and Francis, London, UK, 1993.
11. M. S. Martin-Gonzales, M. A. Garcia, I. Lorite, J. L. Costa-Kramer, F. Rubio-Marcos, N. Carmona, J. F. Fernandez, J. Electroch. Soc., 157 (2010) E31.

Садржај: *Магнетне особине мезоскопских материјала, између осталог, зависе од величине зрна и површинских ефеката. Сол-гел метод је метод којим се могу подешавати величина и окружење. Сол-гел методом су направљени узорци нанокомпозита $Co_{1+y}Al_{2-y}O_4$ наночестица диспергованих у аморфном SiO_2 са различитим масеним уделом спинела $Co_{1+y}Al_{2-y}O_4$ у композиту – x. Масени удео је ишао од претежно SiO_2 (x = 10 wt%) до претежно спинела (x = 95 wt%). Концентрације Co у спинелу $Co_{1+y}Al_{2-y}O_4$ –y, су такође вариране. За узорке са претежно спинел фазом добијене величине зрна спинела су биле испод 100 nm али са великом дистрибуцијом по величинама. Ти узорци су показивали парамагнетизам Кири-Вајсовог типа са антиферомагнетно интерагујућим јонима Co (θ ≈ -100 K). Величина зрна спинела је била испод 100 nm чак и за узорке са само 5 wt% аморфног SiO_2. Код узорака са претежно SiO_2, зрна спинела су раздвојена и величине око 100 nm али се такође могу уочити и знатно мање честице величине око 10 nm. Код тих узорака магнетне особине показују сложенију зависност, долази до прелаза у фазу спинског стакла на најнижим температурама и апсолутна вредност θ је нижа што одговара мањој вредности константе измене.*

Кључне речи: *Магнетни материјали; сол-гел; нанокомпозити; спинско стакло; магнетне особине.*